Geologically calibrated mammalian tree and the corresponding global events, including birth of human

Soichi Osozawa (kawaoso@icloud.com)
Tohoku University https://orcid.org/0000-0001-5554-1320
John Wakabayashi
California State University, Fresno

Research Article

Keywords: mammalian timetree, BEAST v1. X, Pangea, K-Pg boundary, C4 grass, CO2, climatic change, exponentially increased base substitution rate

Posted Date: May 14th, 2021

DOI: https://doi.org/10.21203/rs.3.rs-523676/v1

Abstract

The robust timetree could be constructed using a calibration function of BEAST v1. X released in 2018 simply by applying times of the most recent (= the latest) common ancestors (tMRCAs) for specific monophyletic species groups (clades). The present research is probably the first trial to fully use the calibration function in BEAST X. The specific node age (child tMRCA) in BEAST X = “minimum age” in conventional MCMCTree, but the “maximum age” in MCMCTree can be equivalent to, e.g., the parent node age (parent tMRCA) in BEAST X. We applied 19 mammalian fossil calibration ages considering Benton et al. (2015; solely their minimum ages), including those of fossil *Gorilla* and *Pan* + one geologic event calibration age for otters (= Quaternary isolation time of the Ryukyu islands and start of vicariant speciation), and we estimated our targeted splitting age of *Homo* and *Pan* at 5.69 Ma (calibration dates by Benton et al., 2015 were incorrect). After the initial rifting at 120 Ma, the Atlantic Ocean spread over 500 km on Chron 34 (84 Ma), and Afrotheria (Africa) and Xenarthra (South America) started vicariant speciation at this time (~ 70 Ma), reflecting the progressed continental isolation. Ordinal-level differentiations started just after the K-Pg boundary (66.0 Ma), and this timing reconfirmed that mammalian radiation occurred by rapidly filling the niches left vacant by the non-avian dinosaurs. In addition, we made a base substitution rate vs age diagram using the BEAST X function and showed that the rate exponentially increased and accelerated toward the Holocene, other than having the 55 Ma mild peak reflecting the post K-Pg mammalian explosion. The increased rate might have consequently increased the biodiversity, and extensive adaptive radiation might have ultimately birthed *Homo sapiens*. The basic factor of radiation might be the generation and spreading of C4 grasses since 20 Ma, which has been linked to increasing carbon fixation, decreasing atmospheric CO2 concentrations, cooling Earth, and triggering the Quaternary (2.58 Ma ~) glacier-inter glacier cycle and severe climatic change. Note that Perissodactyla and Cetartiodactyla (Laurasiatheria) feed on C4 grasses (savanna), and Carnivora (also Laurasiatheria) is the predator, also suggesting coevolutions since 20 Ma.

1. Introduction

Modern DNA sequences are an integration of base substitutions, although ancient sequences can be restored using functions such as in MEGA X (maximum likelihood method; Stecher et al., 2020), and recombinant firefly proteins were actually made (Oba et al., 2020). The phylogenetic tree built by application of the DNA sequence is a graphical representation of evolutionary history, and the splits reflect organic populations that diverged and evolved independently. The history or tree is, however, shown on a relative timescale, and an absolutely dated tree is only obtained by calibration applying geologically reliable chronological data on specific nodes. A molecular clock can be used to estimate tree age by assuming typically an approximately constant base substitution rate, and the dated phylogeny can be obtained by such an assumption (e.g., Brower, 1994). However, the molecular clock maintains inaccurate time even in relaxed clocks, as shown in the present paper.

Molecular clock analyses were reviewed by Ho and Duchene (2014), and the concept of geologically determining every node age (= to build a geologically dated tree) was applied to the Bayesian MCMC

method, such as MCMCTree in PALM (4.9e 2017; Yang, 2007) and BEAST. We employed herein the most recent version of BEAST v1. X (v1.10.4 2021; Suchard et al., 2018) with a strictly defined calibration function and protocol for clock analyses. A node calibration is performed by the oldest discovered representative fossil age of the specific clade, which is used to constrain the time of the most recent (= the latest) common ancestor (tMRCA; expression in BEAST) of monophyletic ingroup species. Because the input tMRCA of the specific clade equals the output node age with the same specific clade, the calibration, usually for multiple nodes, can estimate the resting node ages, including ancestor nodes, i.e., reconstruct the topological and chronological relationships across clades. Note that the present research is not “tip dating”, a procedure not yet fully mature (Turner et al., 2017); thus, BEAST 2 (Bouckaert et al., 2014) was not employed for the present analyses.

The software BEAST v1. X and v.1.8 has not been fully used by any researcher except for Oba et al. (2020) and Osozawa et al. (2021ab), although either the dataset or the calibration strategy is novel and clear, which offers the motivation of the present work. See “Fossil calibration protocols: Competition between BEAST and MCMCTree” and Table 1 in the methods section for details, advantages, and innovations to employ BEAST v1. X.

We took the opportunity to re-examine the relationships within whole mammals based on robust and comprehensive molecular phylogenetic analyses for a total of 133 taxa (66 taxa: Primates) with whole mitochondrial sequence data (10,123 bp is available) from GenBank/DDBJ (Figs. 1 and 2). Note that currently employed mitochondrial genes have high resolution compared to nuclear genes, applicable for old age without mutation saturation (Osozawa et al., 2013, 2017c), and paralogs recognized in nuclear genes are unconsidered (Gabaldon and Koonin, 2013). We applied a total of 19 mammalian fossil calibration ages considering Benton et al. (2015; Fig. 2) and one geological event age considering Osozawa et al. (2012a).

No conventional analysis is found for MCMCTree when geological event calibration is applied, and the application example may be solely for BEAST v1. X and MEGA 5 (Osozawa et al., 2013). The geological event should have geological evidence and supporting data, and the event age should also be chronologically robustly dated in the opinion of the present authors. Xenarthra (South America) and Afrotheria (Africa) were expected to have diversified by the Pangea breakup, and Nishihara et al. (2009) addressed the simultaneous divergence by genomic analyses combined with geological constraints related to the breakup age of 120 Ma (second author, Maruyama: geologist). A start date of the breakup of 120 Ma can be applied to the calibration date, but a problem is that animals can disperse across the narrow proto-Atlantic Ocean, and calibration should be done by a date younger than that start age. New World monkeys in South America are supposed to have been rafting on floating islands from Africa at much younger ages than 120 Ma (Houle, 1999).

The above problem is not a case of the formative process of the Ryukyu Islands (Osozawa et al., 2012a). Rifting and sea floor spreading occurred simultaneously over the whole arc of 1000 km, starting everywhere at 1.55 ± 0.15 Ma and quickly subsided and separated each other within this date. Therefore,

vicariant speciation simultaneously started at this time and acted on each isolated island population. The Quaternary time of MRCA at 1.55 ± 0.15 Ma is thus a fixed, robust and reasonable date for geological event calibration as the isolation of each island of the Ryukyu. Based on the prediction by Osozawa et al. (2012a), we have already applied this calibration date as the tMRCA of insect clades (Osozawa K et al., 2016; Osozawa and Wakabayashi, 2015; Osozawa et al., 2013, 2015ab, 2016, 2017abc, 2021ab). These species started vicariance at 1.55 Ma, and each node-specific clade was calibrated by 1.55 ± 0.15 Ma. The present study applied this geologic calibration to the Asian continental and Japan island otters (Waku et al., 2016; Fig. 1, calibration point Z).

The mammalian timetree was constructed by many authors (Bininda-Emonds et al., 2007; Meredith et al., 2011; dos Reis et al., 2012, 2018; O'Leary et al., 2013; Pozzi et al., 2014; Liu et al., 2017). All the above referenced timetrees were motivated to address mammalian ordinal radiation after, across, or before the Cretaceous-Paleogene (K-Pg) boundary (definition after O'Leary et al., 2013), which was related to considering the effect of mass extinction eliminating non-avian dinosaurs. Additionally, some papers tied the superordinal differentiation with the middle Cretaceous supercontinent break-up (Nishihara et al., 2009) and with the Cretaceous angiosperm radiation (Magallon et al., 2015; Liu et al., 2017; Osozawa et al., 2021b). We can now robustly date the mammalian tree (Figs. 1 and 2) and chronologically correlate the biological divergences with the global geological events.

Another topic is related to the sex-determining region Y (SRY) gene, which is responsible for the initiation of male sex determination in therian mammals (Berta et al., 1990); therefore, the root node age represents the original date of the SRY gene. Additionally, placenta is a defining characteristic of placental mammals. The first introgression date may be a node age between Metatheria and Placentalia, although such introgressions were repeated. The protein syncytin, found in the syncytiotrophoblast, has an RNA signature in its genome originating from an ancient endogenous retrovirus that carries out an essential function in placental development (Dupressoir et al., 2012). Syncytin 1 is conserved in all hominoids but has not been characterized in Old World monkeys and lacks in New World monkeys (Caceres et al., 2006). Syncytin 2 is present in Simiiformes and is absent only in prosimians (Blaise et al., 2002). Our timetree correctly shows these evolutionary event dates.

The consequent mammalian timetree calculated by the platform software BEAST was drawn by FigTree. We set BEAUti (associated software in BEAST; see methods section) as selecting relaxed clock model (Ho and Duchene, 2014), and checked variable base substitution rate (rate median of three branches; not constant in a case of relaxed clock model; constant in a case of strict clock model). We made a base substitution rate (rate median) vs age (node age) diagram (Figs. 1 and 2 inset), which indicated that the rate was not random but exponentially increased toward the Holocene, other than having an additional 55 Ma mild peak reflecting mammalian radiation after the K-Pg mass extinction. This phenomenon of exponential increase in the Quaternary has been shown for taxa including primates (Ho et al., 2005, 2011), and we now try to reconfirm and address this basic factor. The implication highlighted that *Homo sapiens* was created by reflecting the accelerated mutation, partly as a consequence of adaptation to local environment change due to the start of East African rifting (Stevens et al., 2013), and mostly as a

consequence of expansion of C4 land grasses (Cerling et al., 1997) triggered global climatic change represented by start of the Quaternary glacial-interglacial cycle (Taira, 2007). Taira (2007) also pointed out that the C4 savanna was tied to Laurasiatheria evolution. We can also precisely estimate the splitting age between *Pan* and *Homo* from our newly dated tree.

2. Methods

2.1. Phylogenetic analyses by BEAST v1. X: General

A Bayesian inference (BI) tree (Fig. 1) was constructed using the software BEAST v.1 X, running BEAUti, BEAST, TreeAnnotator, FigTree, in ascending order. BEAGLE Library must be priorly downloaded to operate platform software of BEAST. Tracer v.1.6 was applied to check the calculation status and estimate the mean base substitution rate.

With graphic explanation, see “BEAST v1. X tutorial: Mammalian timetree” in protocols.io:

dx.doi.org/10.17504/protocols.io.brdym27w

2.2. Applied whole mitochondrial sequence: Competition between BEAST and MCMCTree (Table 1)

We used uploaded whole mitochondrial sequence data of most primates and representative mammals analyzed by Pozzi et al. (2014), and the accession numbers are shown in Fig. 1. In addition, we sought other representative mammalian data covering every order available from GenBank/DDJB and included them in our BEAST analyses.

The whole mitochondrial sequences were aligned by ClustalW in MEGA X. Gapped areas of nonprotein cording regions were excluded from the aligned sequences, and the consequent protein cording sequence data had a total of 10,112 bp. Concatenating of genes by SeaView (Gouy et al., 2010) and further partitioning by PartitionFinder 2 (Lanfear et al., 2016) in MCMCTree analyses is not needed in the present BEAST analyses, and the 10,112 bp sequence represents a single long partition.

2.3. Fossil calibration protocols: Competition between BEAST and MCMCTree (Table 1)

To estimate the evolutionary rate, calibration is essentially necessary, and fossil and geological event calibration is possible (Ho and Duchene, 2014). A node calibration is by the oldest discovered representative fossil of the specific clade, and the fossil is used to constrain its “minimum age” (Donoghue and Yang, 2016). Due to the fragmentary nature of the fossil record and the oldest fossil relying on negative evidence, the true MRCA of a clade will likely never be found.

For the mammalian fossil calibration in the MCMCTree, however, both the minimum and maximum age constraints for a specific node were proposed (Benton and Donoghue, 2007). The minimum age is

expected to be the oldest fossil age younger than the specific branch node within the clade. The maximum age is inferred by an additional fossil age older than that specific node (and the minimum age), i.e., the stem age (or the parent node age at an edge) is representative, although the definition is sometimes unclear and controversial. Minimum ages are generally more accurate and reliable than maximum ages (Hassanin et al., 2021). In actual mammalian MCMCTree analyses (dos Reis et al., 2012, 2018), a specific node age (posterior divergence time) is estimated by prior divergence time applying minimum and maximum ages, although maximum age is only roughly estimated (named soft maximum bound). A root node age for the tree = the oldest maximum constraint as the third fossil age, is demanded for the algorithm to converge on a unique solution in MCMCTree.

Calibration protocol of BEAST v1.X. (and v.1.8) is to input a time of the most recent common ancestor (tMRCA) of the ingroup species (clade) on that specific node, and we can approximate the tMRCA to the single, oldest fossil age known at the time of analyses. The minimum ages proposed by Benton et al. (2015) for MCMCTree coincident with our tMRCA for BEAST X, and the maximum age does not need to be constrained in BEAST X. A root node age in the MCMCTree analyses is simply equivalent to the tMRCA of the root node in BEAST X, and a third fossil age is not needed (the root age should be applied or automatically estimated from the resting child tMRCAs). Note that the BEAST v.1 X and v.1.8 protocol was drastically changed from BEAST v.1.7 with a similar calibration protocol in MCMCTree (several developers are common in these software programs).

We now awake that both BEAST and MCMCTree input prior node ages and output posterior node ages are expected to be coincident. The difference is that the BEAST node age (tMRCA) is younger than the MCMCTree node age, such as the mean (maximum age + minimum age)/2 by standard deviation (maximum age – minimum age)/2, and that the output time tree by MCMCTree as a whole may extend and shift to older dates relative to that by BEAST. Namely, if MCMCTree inputs the same prior node ages as BEAST in the same fashion, it outputs the similarly dated tree as BEAST. The difference may be the calibration protocol considering maximum age or not, and we tested below the effect of applying tMRCA as minimum age or (maximum age + minimum age)/2 (Figs. 3 and 4). Phillips (2016) pointed out that tight calibration across the tree is vital to buffer against rate model errors, and this must include allowing maximum ages to be tight when good fossil records permit.

We employed a normal prior distribution, but the selection of a lognormal distribution may affect node dating (Phillips, 2016), and we also tested and compared these two prior distribution settings (Fig. 5).

We noted above which is the oldest relevant fossil within the clade is in question. Our choice is BEAST analyses including the above testing, and we consider that tMRCA equals the oldest discovered representative fossil age of the specific clade or the oldest fossil age known at the time of analyses. In the future, if new fossils with older dates may be found, the calibration date should only be modified to older dates. Note that famous fossil localities, such as the Burmese amber, are restricted, and the age has recently been well constrained by the efforts of paleontologists and geochronologists, but finding new fossil localities with excellent preservation on Earth may not be easy. The present timetree was made by

robust calibration by a total of 20 multiple points covering 0.545 Ma (Quaternary) up to 162.7 m.y. (Jurassic), and the dated tree is balanced or equilibrated (if not, some branch is folded in the ultimate case in the output figure by FigTree) and finally established. The run time BEAST was more than 5 hours for the present long sequence data, but we needed dozens of runs to obtain a finalized mammalian dated tree. Repeated runs are a problem for command line software such as MCMCTree.

Note that multiple calibration points are particularly helpful in relaxed-clock methods where the rate is allowed to vary among branches in the tree; multiple calibrations throughout the tree act as anchor points, allowing the method to estimate the patterns and degree of rate variation more accurately. Good estimates of rate variation are required from the well-calibrated regions of the tree so that the pattern can be extrapolated to other parts of the tree that are poorly calibrated (Phillips, 2016). In this meaning, the maximum age in MCMCTree can be replaced by the age of the parent node at a step from the specific child node with tMRCA in BEAST v1. X.

The fossil age should be chronologically checked strictly following the protocol proposed by Parham et al. (2012), which is geologically robust in the opinion of the present authors. Reliable radiometric age by Ar-Ar or U-Pb radiometric dating is recommended, and the age is represented by 98.79 ± 0.62 Ma for the fossiliferous Burmese amber (although no mammalian fossil). In some cases, fossil ages are represented, such as Cenomanian (97.2 ± 3.3 Ma) of chronostratigraphic unit. Ages are after International Chronostratigraphic Chart by International Commission on Stratigraphy (2013).

2.3. Actual fossil calibration dates

Calibrations were as follows: the points of prior (input) ages (tMRCAs) are shown in Figs. 1 and 2 green stars, and these dates were input in “Priors” in BEAUti as the mean and standard deviation (in the case of 98.79 ± 0.62 Ma, mean = 98.79, standard deviation = 0.62). Corresponding ingroup species (clade) were included in ingroup taxa by “Taxon Set” on “Taxa” screen in BEAUti.

Figures 3 and 4 were made by prior (input) age of mean: (maximum age + minimum age)/2 and standard deviation: (maximum age – minimum age)/2, in the similar fashion to MCMCTree for testing the affect concerning maximum age. However, note that MCMCTree dating may be statically much more complex. Figure 5 reflects a prior lognormal distribution (Figs. 3 and 4 reflect a normal distribution).

Ingroup species or clade species are monophyletic (a function of BEAUti), although a clade species is obviously monophyletic. This treatment is for confirmation of Afrotheria species should be included in the Afrotheria clade, for example. For convenience in selecting ingroup taxa, we offered headings such as “Afro” in the sequence file. We checked the stem (a function of BEAUti) for four ingroup species (Prototheria, Theria, Bovidae, Eulipotyphla) because the fossil age is explained to not represent tMRCA (within the clade) but its stem (Fig. 2).

Our fossil calibration points were 19 points in total and covered long datums from 0.545 to 162.7 Ma (root age; 162.7 Ma). In every case, we referred to the original study, performed an additional literature search to find chronological evidence of the data, and modified the age. In Figs. 1 and 2, we show fossil

calibration points from A to S with the prior input age, but calibration point Z is determined by geological event calibration at 1.55 ± 0.15 Ma (then totally 20).

Benton and Donoghue (2007) and Benton et al. (2015) reviewed many calibration data available for animals, and the following mammalian calibration points and dates are addressed by their proposal, except for calibration point X, which cannot be applied, and K, which we ourselves offered. These data were for MCMCTree analyses, and the maximum ages by Benton et al. (2015) are also addressed below to construct Figs. 3 and 4. In Figs. 2 and 4, fossils to adjust minimum ages (= times of MCRA) are also shown (Benton et al., 2015). In Fig. 6, we show our point node ages of A to E and X compared with the corresponding broad node ages by Benton et al. (2015).

Calibration point A: Fossil chimpanzee was reported from the East African Rift and dated by the Ar-Ar method as 0.545 ± 0.003 Ma (McBrearty and Jablonski, 2005). The time of MRCA is a node date between two *Pan* species (Fig. 1), although Benton et al. (2015) cited only the above reference and did not address the chimpanzee split. We here set the maximum age at 5.31 ± 0.03 Ma of the calibration point X below.

Calibration point X: Crown Hominini (87) by Benton et al. (2015); Not applied in this paper because chronological evidence was not enough. Benton and Donoghue (2007) and Benton et al. (2015) noted that in the Lukeino Formation of Kenya, the source of *Orrorin* (Hominina) was dated at 6.56–5.73 m.y. from Ar/Ar ages on volcanic layers, citing Deino et al. (2002). The Lukeino Formation at Kapcherberek, including the fauna, was deposited during chron C3r and can be constrained to the interval 5.88–5.72 Ma (Deino et al., 2002), but this correlation to the magnetic polarity timescale is uncertain. Ar/Ar dating with an age of 5.31 ± 0.03 Ma (Deino et al., 2002) is only available for the ignimbrite and associated air-fall tuff of the basal Chemeron Formation, not the overlying Lukeino Formation. The age constraint for *Orrorin* loclity is thus only before 5.31 ± 0.03 Ma, and no evidence of lower limit of 6.56 Ma. In addition, Benton and Donoghue (2007) and Benton et al. (2015) noted that dating of the *Sahelanthropus* (oldest Hominina) beds in Chad is indirect. According to them, biostratigraphic evidence from mammals in particular, but with cross-checking from fish and reptile specimens, only indicates that the unit is definitely late Miocene (i.e., older than 5.33 m.y.). It is older than the Lukeino Formation of Kenya (thus older than 5.31 ± 0.03 Ma) and may be equivalent (biostratigraphically correlated) to the lower fossiliferous units of the Nawata Formation of Kenya (dated by the traditional K-Ar method as diverse and unreliable ages of 7.4 and 6.5 Ma; Vignaud et al., 2002). Therefore, crown Hominini age is not constrained or only > 5.31 ± 0.03 Ma, and we did not adopt point X for our calibration or prior setting. Conversely, we tried to estimate node X age from the other reliable calibration data. Maximum age at 12.72 ± 1.1 Ma is for *Sivapithecus* at calibration point C below according to Benton et al. (2015), not 8.072 ± 0.8 Ma for *Chororapithecus* at calibration point B below (see Fig. 6), although we did not employ these dates to our calibration point X.

Calibration point B: Fossil gorilla (*Chororapithecus abyssinicus*) was also reported from the East African Rift and combined with the Ar-Ar method and megnetostratigraphy, reliably dated at 8.072 ± 0.8 Ma(Katoh

et al., 2016). The time of MRCA is a node date of Homininae (*Gorilla*, *Pan*, and *Homo*). We set maximum age at 12.72 ± 1.1 Ma for *Sivapithecus* in calibration point C below.

Calibration point C: Crown Hominoidea; great apes (86) by Benton et al. (2015). *Sivapithecus* (Ponginae) fossil was found in Pakistan and considered to be the Serravallian stage (12.72 ± 1.1 Ma). Benton et al. (2015) proposed a minimum age of 11.62 (12.72–1.1) Ma, and the maximum age is a stem date of fossil Ponginae placed at the base of the Oligocene (33.9 Ma). However, the maximum age at 33.9 Ma should be replaced by younger node D age at 24.93 ± 0.49 Ma (see Fig. 2).

Calibration point D: Crown Catarrhini (Cercopithecoidea; Old World monkeys + Hylobatidae + Hominoidea) (84) by Benton et al. (2015). The Nsungwe Formation, Tanzania, contains *Rukwapithecus*, and the U-Pb age is 24.93 ± 0.49 Ma (Roberts et al., 2010; Stevens et al. 2013). Benton et al. (2015) proposed a minimum age of 24.44 (24.93–0.49) Ma, and the maximum age is on a stem of fossil Catarrhini placed at the base of the Oligocene (33.9 Ma).

Calibration point E: Crown Primates; Primates (81) by Benton et al. (2015). Fossil *Altiatlasius* (euprimate) was found in Morocco and considered to be the Thanetian stage (57.6 ± 1.6 Ma). Maximum age at 66.0 Ma is from the Danian primate fossil.

Calibration point F: Crown Euarchonta; Euarchontoglires (74) by Benton et al. (2015), but we excluded the Glires clade to contain Scandentia in the Euarchonta clade (if not, Scandentia becomes the basal clade of Euarchontoglires). Fossil *Paromomys* (Primates, not Euarchontoglires) were found in Montana, USA, and considered to be the Danian stage (63.8 ± 2.2 Ma). The maximum age was the same as the tMRCA of calibration point R: Crown Theria (59) by Benton et al. (2015) and *Juramaia sinensis* from Liaoning, Northeastern China, with an Ar-Ar age of 160.7 ± 0.4 Ma (Luo et al., 2011). This too old date compared to the minimum age may not constrain the dating.

Calibration point G: The common ancestor of Lagomorpha (Leporidae; leporids; rabbits and hares + Ochotonidae; ochotonids; pikas) (76) by Benton et al. (2015). The Indian leporid fossil horizon was considered to be the Yepresian (51.96 ± 4.6 Ma) based on the foraminifer zone (Rose et al., 2008), and the tMRCA of Lagomorpha equals the stem age of Leporidae at 51.96 ± 4.6 Ma. Maximum age is 66.0 Ma (K-Pg boundary) from Glires fossil.

Calibration point H: Crown Rodentia (77) by Benton et al. (2015). Fossil *Paramys* was found in Montana, USA, and considered to be the Thanetian stage (57.6 ± 1.6 Ma). Maximum age: same as above 66.0 Ma. We did not apply Crown Glires (75) by Benton et al. (2015) (77) by Benton et al. (2015) because the age of the Wanghudun Formation with *Mimotona*, China, is uncertain.

Calibration point I: Intra-Murinae, Divergence of *Mus* from *Rattus* (79) by Benton et al. (2015). The fossil (*Karnimata*) horizon, Pakistan, was stratigraphically, magnetostratigraphically, oxygen isotopically dated at 10.4 Ma (Barry et a., 2002). The age of fossil *Antemus*, Pakistan, as a maximum age, is not chronologically constrained.

Calibration point J: Crown Carnivora (69) by Benton et al. (2015). The fossil *Hesperocyon* was from the Canadian Duchesnian with radiometric age (Robinson et al., 2004) and estimated at 37.8 ± 0.5 Ma. Maximum age is 66.0 Ma (K-Pg boundary) from Carnivora stem fossil.

Calibration point K: *Orohippus* (Equidae) was reported from the Green River Formation, USA (Grande, 1980). Ar-Ar dating applied to the silicic tuff within the formation yields ages of 53.5–48.5 Ma (weighted average of 51.25 ± 0.31 Ma; Smith et al., 2003). Although *Orohippus* evolved from equids such as *Eohippus*, we used the above data for our calibration for Perissodactyla + Carnivora. Bat (Phyllostomidae) fossils, as well as primate fossils, were also reported from the Green River Formation (Grande, 1980), and bats (not calibrated) are included in our timetree with similar output node ages (Fig. 1).

Calibration point L: Crown Bovidae = Divergence of Bovinae (cow) and Antilopinae (sheep) (73) by Benton et al. (2015). The fossil (*Pseudoeotragus*) horizon in the Siwalik Deposits is the Burdigalian stage (18.205 ± 2.235 Ma) based on the paleomagnetic chronology (Johnson et al., 1985). Maximum age is Chattian (25.425 ± 2.395 Ma) from the Bovidae stem fossil.

Calibration point M: Crown Artiodactyla (70) (part of Cetartiodactyla) by Benton et al. (2015). The fossil (*Himalayacetus*) horizon, Pakistan, was correlated to the planktonic foraminifer zone, and 53.25 ± 0.75 Ma (Bajpai and Gingerich, 1998). Maximum age is considered at 66.0 Ma (K-Pg boundary).

Calibration point N: Crown Eulipotyphla (68) by Benton et al. (2015). Fossil *Adunator* was found in Montana, USA, and considered to be the Danian stage (63.8 ± 2.2 Ma) considered as the stem age. The maximum age is the same as the above *Juramaia* age of 160.7 ± 0.4 Ma.

Calibration point O: Crown Afrotheria (63) by Benton et al. (2015). Fossil *Eritherium* was found in Morocco and considered to be the Thanetian stage (57.6 ± 1.6 Ma). The maximum age is the same as the above *Juramaia* age of 160.7 ± 0.4 Ma.

Calibration point P: Crown Xenarthra (62) by Benton et al. (2015). Fossil *Ristegotherium* was found in Brazil and considered to be the Thanetian stage (57.6 ± 1.6 Ma). The maximum age is the same as the above *Juramaia* age of 160.7 ± 0.4 Ma.

Calibration point Q: Crown Marsupialia (58) by Benton et al. (2015). Fossil *Djarthia* was found in Murgon, Australia, and considered to be the Yepresian stage (51.96 ± 4.6 Ma). The maximum age is from fossil *Sinodelphys* described from the Jehol Biota, Liaoning, northern China (Luo et al., 2003). The intercalated silicic tuff was dated by the Ar-Ar method, and the obtained age was 130.7 ± 1.4 Ma (He et al., 2006).

Calibration point R: Crown Theria (59) by Benton et al. (2015). *Juramaia sinensis* from Liaoning, Northeastern China, with an Ar-Ar age of 160.7 ± 0.4 Ma corresponding to the Oxfordian (Luo et al., 2011). Benton et al. (2015) sets the maximum age at 162.7 ± 1.1 Ma from the *Ambondro* fossil below.

Calibration point S: Crown mammalia (57) by Benton et al. (2015). *Ambondro mahabo* from Madagascar is placed within Monotremata and considered to be the Bathonian stage (162.7 ± 1.1 Ma). The maximum

age was assumed to be the Jurassic-Triassic boundary at 201.3 Ma.

2.4. Recovering ancient base substitution rates

The consequent mammalian Bayesian Inference tree calculated by the platform software BEAST was drawn by FigTree. We set BEAUti (associated software in BEAST) to select a relaxed clock model (Ho and Duchene, 2014) and checked the variable base substitution rate (rate median of three branches; not constant in the case of a relaxed clock model) in the output tree by FigTree.

We made a base substitution rate (rate median) vs age (node age) diagram (Figs. 1 ~ 5 inset) from the data on the output tree. An approximate curve with its formula is shown on this diagram using the Excel function. The intersection for the curve was 0.0114, the rate median shown on Tracer, in the case of Figs. 1 and 2 inset.

3. Results

3.1. Maximum ages unaffected on dating

Figures 1 and 2 were constructed by calibration by input tMRCA = minimum age, and Figs. 3 and 4 were constructed by calibration by input tMRCA = (maximum age + minimum age)/2. In Figs. 3 and 4, the output dates are not affected by the maximum ages but equal to the input minimum ages, as in Figs. 1 and 2. These two kinds of trees then become similar, unrelated to the two kinds of calibrations. A difference is longer 95% HPD (height posterior density) in Figs. 3 and 4 compared to Figs. 1 and 2 (these bars were not shown in these figures to avoid complexity). Eventually, overestimated maximum ages caused too large and unreasonable standard deviations found at calibration points C, F and N ~ R but did not affect the dating, i.e., the timetree was strongly affected or controlled by the resting calibration points with negligible standard deviations. A minor difference is only that Xenarthra is a sister or not a sister of Afrotheria, but superorder level differentiation almost simultaneously occurred before the K-Pg boundary, common to Figs. 1 and 2.

Figure 5 is a timetree made by the same BEAUti setting as Figs. 3 and 4 but changed to a prior lognormal distribution, but the dating and topology are similar to Figs. 3 and 4.

3.2. Mammalian timetree and differentiation

We previously set superorder- to grandorder-level clades with their tMRCAs except for the Glires clade in BEAUti, and the relation of these superorder clades was reasonably restored in Figs. 1 and 2. Prototheria is the basal clade at 160.97 Ma, Metatheria is next at 94.66 Ma. Placentalia were differentiated into superorder clades since 73.42 Ma, and these superorder clades were thereafter differentiated into grandorder ~ species level clades. The relation of grandorder ~ species level clades was reasonably restored in Figs. 1 and 2 by ancestor to descendant node calibrations.

Placentalian superorder level differentiation dates were estimated before the K-Pg boundary (66.0 Ma) except for Euarchontoglires clade at 65.64 Ma. Because prior tMRCAs of Placentalia superorder clades were set younger than 66.0 Ma (K-Pg boundary), all the order-level differentiations were post-K-Pg boundary followed by family-level differentiations.

For great apes, *Pongo* was differentiated from other great apes at 13.4 Ma. *Gorilla* was differentiated from *Pan* and *Homo* at 8 Ma. *Homo sapiens* was estimated to have differentiated from *Pan* at 5.69 Ma (target age), *Homo sapiens* ssp. *Denisova* was differentiated from *Homo sapiens neanderthalensis* and *Homo sapiens* at 2.09 Ma, and *Homo sapiens neanderthalensis* was differentiated from *Homo sapiens* at 0.95 Ma.

3.3. Inconsistent Mammalian base substitution rate

The base substitution rate vs age diagram (Figs. 1 ~ 5 inset) shows that the rate was not constant and exponentially increased toward the Recent from ca. 20 Ma, and the heavy red trendline and equation using the Excel functions are shown on the inset.

The light red fluctuation curve was drawn by connecting maximum rate points over time and has a broad peak at approximately 55 Ma, delayed from the K-P boundary at 66.0 Ma (Figs. 1 ~ 5 inset).

4. Discussion

4.1. Placental ordinal radiation after the K-Pg boundary

Three diversification models of extant placental mammals were proposed with respect to the K-Pg extinction event (Archibald and Deutschman, 2001), and in short, the inter ordinal (not superordinal) diversifications were in the Paleogene (after the K-Pg boundary; explosive model), across the K-Pg boundary (long fuse model), and in the Cretaceous (before the K-Pg boundary; short fuse model) (the clearest definition; O'Leary et al., 2013). These models were reviewed and modified by Phillips (2016), Liu et al. (2017), and Spronger et al. (2019), but the definition tends to become rather controversial, and the factor of the short fuse model has not been addressed.

Although superorder level diversifications for Xenarthra, Afrotheria, Laurasiatheria, and Euarchontoglires were at pre K-Pg 73.42, 71, 68, and post K-Pg 65.64 Ma, all the order level (grandorder ~ infraorder level) diversifications occurred after the K-Pg boundary (Figs. 1 and 2), and this fact supports the explosive model. The explosive model predicted that the ordinal radiation of present-day mammals occurred just after the K-Pg boundary was triggered by the mass extinction event eliminating non-avian dinosaurs and most of the end-Cretaceous fauna.

O'Leary et al. (2013) proposed the explosive model by constructing a timetree that emerged from the combined phenomic and molecular parsimony analyses for fossil and living species. They applied multiple fossil ages for the oldest members of the clades to their timetree to determine the minimum divergence dates, and the fossil minimum ages were directly affected on their timetree. We confirmed that

only maximum ages did not affect our timetree, but minimum ages were directly affected (Figs. 1 and 2 vs Figs. 3 and 4).

In the following studies, except for older ones, calibration dates were after Benton et al. (2015), and the employed software was MCMCTree (Yang, 2007). The mammalian timetrees by dos Raise et al. (2012), Wu et al. (2017), and Liu et al. (2017) agreed with the long fuse model, and ordinal differentiations crossed the K-Pg boundary (66.0 Ma). Ordinal differentiation of the pre- or post-K-Pg boundary is critical, and we checked the effect of the calibration described in dos Raise et al. (2012). Affected by marginal prior density of divergence times in MCMCtree analyses (their Fig. 3), the 12 node calibrations solely by minimum ages (lacking maximum ages) estimated the posterior ages (= posterior density in their Fig. 3) older than the minimum ages, approximate to the presumed maximum age (predicted in MCMCTree but conflict with ours). Therefore, for these 12 node calibrations, the lack of maximum age data produced unexpected older node age estimates that explained the long fuse model. Note that 11 node calibrations both by minimum and maximum ages and 2 node calibrations by solely maximum age put the posterior ages between the minimum and maximum age, as we predicted (but in BEAST analyses, close to the minimam ages as shown by Figs. 3 and 4). MCMCTree analyses actually need to include maximum age data to avoid this disadvantage and obtain accurate timetree, but our opinion is that overestimated maximum ages should be eliminated from dating analyses such as in BEAST v1. X. Application of genome-scale sequence data may be better as dos Raise et al. (2012) did so, but in the present case unrelated to the precision of node dating, calibration method is much more important.

Hassanin et al. (2021) applied a lognormal distribution on the calibrated node ages and compared it to the uniform distribution for the minimum and maximum age sets. In BEAST v.1 X, considering maximum ages, we tried to select lognormal for prior distribution to construct Fig. 5 and compared to the normal distribution constructing Figs. 3 and 4. Our trial showed that posterior node ages close to the minimum ages (unaffected by too large standard deviation data) were not controlled by the prior lognormal distribution (Fig. 5), and the discrepancy was not from this distributional setting.

The timetrees by Bininda-Emonds et al. (2007), Meredith et al. (2011) Pozzi et al. (2014; Multidivtime; Thorne and Kishino, 2002) accord with the short fuse model. The discrepancy may also be related to considering the maximum ages in their dating analyses, but dos Raise et al. (2012) did not address the reason for discordance with Bininda-Emonds et al. (2007).

4.2. Relation to the middle Cretaceous Pangea breakup

In Eutheria (Placentalia), divergence into Afrotheria, Xenarthra, and Boreoeutheria (Laurasiatheria + Euarchontoglires) was considered to be tied to major-scale vicariant speciation by the breakup of the supercontinent Pangea into Laurasia (Eurashia and North America) and Gondwana (Africa and South America). Although the factor of differentiation into Laurasiatheria and Euarchontoglires has not been addressed, we tentatively assume that Laurasiatheria originated in North America (named the Laurentia continent) + Europe and that Euarchontoglires originated in Eurasia – Europe in the following discussion. The phylogenetic basal split was considered to have followed the order of continental division between

100 and 120 Ma (Murphy et al., 2001). Nishihara et al. (2009) geologically estimated the date of the Gondwana breakup and proposed simultaneous divergence at approximately 120 Ma. The age of the fossiliferous Santana Formation, Brazil, is coeval with the breakup and initiation of the Atlantic Ocean and may be Aptian, Albian or possibly Cenomanian, although a rather loosely constrained date (125 – 100 Ma; Martill, 2007).

Reports of dos Raise et al. (2012) and O'Leary et al. (2013) rejected the possibility of major-scale vicariance; the crown age of Eutheria (Placentalia) was less than 90 Ma, much younger than the above 125 – 100 Ma break-up. We also do not accept the possibility of relation to the Pangea break-up; crown age of Eutheria (Placentalia) was 73.42 Ma, Xenarthra at 57.26 Ma, and Afrotheria at 57.44 Ma, much younger than the break-up age. However, the factor of Placentalia superordinal differentiations since 73.42 Ma (Figs. 1 and 2) has been remained unsolved.

The initial rifting and seafloor spreading were complex processes to address the starting age mentioned above. However, marine magnetic anomalies on the Atlantic Ocean floor easily reconstructed the periodic spreading history. The configuration at Chron 34 (84 Ma) after the Cretaceous magnetic quiet zone (long normal polarity epoch; superchron K-T at 118 – 84 Ma) was shown by Moulin et al. (2010), and the South Atlantic Ocean spread over 500 km (minimum distance between Africa and South America) at Chron 34 (84 Ma). Therefore, 84 Ma can be considered to be a starting date of continent-level vicariance and divergence between Afrotheria and Xenarthra, which might have triggered the Placentalia superordinal differentiations shown in Figs. 1 and 2.

The splitting date of Lorisiformes (Africa and Southeast Asia) and Lemuriformes (Madagascar) was estimated at 51.23 Ma and unrelated to the initial break-up, but Lemuriformes in Madagascar is considered by oceanic dispersal from Africa (Horvath et al. 2008). We estimated the divergence time of New World monkeys and Old World monkeys to be 43.21 Ma, and the probable dispersal mechanism was proposed to be rafting on floating islands from Africa to South America (Houle, 1999).

The Panama arc docked and emerged with the Andean arc with crust fracturing during collision with South America (Ferris et al., 2017), and the Central American Seaway that did the Caribbean-Pacific water exchange was closed to form the Panama isthmus. The date was indirectly assumed to be the late Oligocene (25 Ma) from exhumation indicated by (U-Th)/He and fission track thermochronology coupled with geochemical changes in Panama arc magmatism (Farris et al., 2011), to be the middle Miocene (13 ~ 15 Ma) from U-Pb ages of magmatic detrital zircons included in the northern Andean frontal basin (Montes et al., 2015) and to be the middle Miocene (18 Ma) from Ar-Ar ages of ignimbrite (Buchs et al., 2018). This date is concerned with the Great American Biotic Interchange and the vicariance of shallow marine organisms between the Atlantic and Pacific Oceans (Bacon et al., 2015). They demonstrated significant waves of dispersal of terrestrial organisms at approximately ca. 20 and 6 Ma and corresponding events separating marine organisms in the Atlantic and Pacific oceans ca. 23 and 7 Ma.

The divergence of Laurasiatheria relative to Xenarthra is possibly related to the partial Pangea breakup into North and South America, i.e., the initial formative time of the Central American Seaway. Marine

magnetic anomalies on the Atlantic Ocean floor constrain the ancient relative position of North and South America, but the Caribbean lithosphere obscures the presence of the Central American Seaway. According to Pindell et al. (2011), a proto-Greater Antillean arc was formed along the Pacific side of Central America by entrapping the Caribbean seaway and connecting North and South America ca. 130 Ma, and the seaway was always narrow (maximum: 1000 km) constrained by the present position and distance of 1000 km between North and South America. The Panama arc is younger than 60 Ma (Montes et al., 2015), and the arc is almost connected to South America. Therefore, the Central American Seaway was not wide enough to diverge Laurasiatheria by vicariance within North America, and its origin cannot be addressed.

For Euarchontoglires relative to Laurasiatheria, the northern Atlantic Ocean associated with the Iceland hotspot initiated final spread since chron 24 (53.3 Ma) after multiple phases of extension (Barnett-Moore et al., 2018). However, seaway was lacking on chron 24 except for older narrow ones, and vicariance was not expected for the connected supercontinental masses.

For Euarchontoglires relative to Afrotheria, the Atlantic marine magnetic anomalies also constrain the position of Europe and Africa, and the Gibraltar acted as the anchor point of the western end of these continents. The Mediterranean Sea and Tethys Sea ended at the Gibraltar Strait and connected Europe and Africa. The Euarchontoglires origin cannot be addressed by vicariance. Closure of the Tethys Sea was related to formative process of European Alps (apatite and zircon fission track ages; exhumation around 15 Ma; Bertrand et al., 2017) and Himalayan Range by Indian collision (exhume episode; the South Tibetan Detachment System; around 20 Ma; Searl and Godin, 2003; gneissose and granitic domes in northern Vietnam; around 25 Ma; Osozawa et al., 2015), and the Semail ophiolite (95 Ma including the age of metamorphic sole; Cowan et al., 2014; Rioux et al., 2021; Arabian Peninsula was a part of Africa; Zagros suture granitoid; U-Pb age: 37.7 ± 1.0 Ma; Rezaei et al., 2021) and the Troodos ophiolite (90, 75, 55 Ma; Osozawa et al., 2012b) also record the closure time, and these closing times may be related to the dispersal events of Afrotheria (or Euarchontoglires).

For Euarchonta, a component of Euarchontoglires, Scandentia (Southeast Asia) and Dermoptera (Southeast Asia) are the oldest lineages, Lorisiformes (Africa and Southeast Asia) is sister to Lemuriformes (Madagascar), and Tarsiiformes (Southeast Asia) is sister to Simiiformes, including New World monkeys. As we calibrated using crown Primates date (81) by Benton et al. (2015), the oldest fossil Primates were from the Thanetian, Morocco, as calibrated at 57.6 Ma. The origin of Euarchonta was Southeast Asia and Africa, but the Euarchontoglires definition becomes unclear.

In Metatheria, *Dromiciops gliroides* is known from Patagonia, South America, but is included in Australidelphia. In the timetree by dos Raise et al. (2012), this species occupied the basal lineage of Australidelphia (pre K-Pg) and a sister relationship with *Notoryctes typhlops* in Fig. 1 (only 21.27 Ma in Fig. 1; 33.12 Ma in Fig. 3). Nilsson et al. (2010) showed a single marsupial migration from South America to Australia by their phylogenetic study including *D. gliroides.* Patagonia, the Scotia arc, and the Antarctic Peninsula originally connected and formed a long land bridge because the Drake Passage was formed by

the Scotia plate spreading after chron C11n (30 Ma; Riley et al., 2019). Therefore, marsupial migration occurred via Antarctica through the long bridge before 33 Ma and dispersed Australia before 33 Ma when the Tasman Gateway initiated opening (Lagabrielle et al., 2009).

As we applied tMRCA of the Asian continental and Japan island otters at 1.55 Ma, isolation of the Japanese island from the Korean Peninsula by the Tsushima Strait (Osozawa et al., 2012) triggered vicariant speciation on isolated populations in Japan. This process is unrelated to dispersal to Japan, especially through land bridges and subsequent vicariance, although recently found otters on Tsushima Island in 2017 were probably dispersed from the Korean Peninsula by swimming. Similarly, we did not calibrated by 1.55 Ma for wildcat (*Prionailurus bengalensis euptilurus*) on Tsushima Island (lacking on the Japan main islands) because relatively recent dispersal from Korea is plausible.

4.3. Relation to the middle Cretaceous Angiosperm radiation

Angiosperms were diversified and radiated in Middle Cretaceous time (Magallon et al., 2015; Osozawa et al., 2021b; approximately 125 Ma), and insect beetles have been clarified to have contemporaneously co-radiated around middle Cretaceous time (McKenna et al., 2015). Mammalian ordinal radiation occurred after the K-P boundary (66.0 Ma) and unrelated to middle Cretaceous angiosperm radiation.

4.4. Physiological evolutionary aspects

The SRY gene is a male sex determination in Theria (Berta et al., 1990), and the mammalian root node age is estimated at 160.97 Ma, and this date represents the origin date of the SRY gene. The origin date of the placenta was a Theria crown age of 94.66 Ma, defining characteristic of placental mammals. The origin date of Syncytin 1 is a crown age of Simiiformes and is estimated at 35.58 Ma. Syncytin 1 is inactive in Old World monkeys, and the inactive date is a crown age of Catarrhini, estimated at 25.2 Ma. Syncytin 2 is found in Simiiformes, and the date is a crown age of Primates, estimated at 57.14 Ma.

4.5. Expanded C4 grasslands and Catarrhini radiation

The calibration of crown Catarrhini was from the African fossil age at 24.93 ± 0.49 Ma (Roberts et al., 2010). Stevens et al. (2013) suggested a possible link between diversification of Catarrhini and the prominent East African rift system, uplift of the African plateau, and the consequent climate and environmental changes. If acceptable, Catarrhini was generated in East Africa. However, Hylobatidae and fossils are known from Southeast Asia, including China (Benton et al., 2015).

The East African uplift led to a drastic reorganization of atmospheric circulation, engendering strong aridification since ca. 8 Ma (Sepulchre et al., 2006). The consequent progressive increase in open grassland was linked to African Hominidae evolution. We estimated crown age of gorilla at 8.38 Ma as calibrated by point B of 8 Ma (Fig. 1). This fact may support the hypothesis of *in situ* African evolution of the *Gorilla*–*Pan*–human clade (Katoh et al., 2016). However, Ponginae is native to the rainforests of

Indonesia and Malaysia, and *Sivapithecus* (Ponginae) fossils were found in Pakistan (Benton et al., 2015).

Quaternary glaciations may have been triggered by the expansion of land grasses (Poales) because this process increased carbon fixation, which consequently decreased atmospheric CO2 concentrations (Taira, 2007). C4 plants are efficient for CO2 fixation (Taira, 2007), and C4 Poales plants appeared and started diversification at 20.35 Ma (C4 dicots from 31.92 Ma) by our Angiospermae timetree (Osozawa et al., 2021b). Carbon isotope ratios from mammalian fossil tooth enamel show that diet change into C4 plants started at 9.9 Ma in eastern Africa (Uno *et al*., 2011). Additionally, the mammalian fossil tooth from the sub-Himalayan Siwalik Group, Pakistan, suggests that C4 savanna replaced C3 forest and woodland between 8.5 and 6.0 Ma (Badgley et al., 2008). The expansion of C4 grasses was a global phenomenon, including North America and South America beginning in the late Miocene and persisting to the present day, and generated the glacial–interglacial period (Cerling et al., 1997). This event should have affected Hominidae radiation as well as Laurasiatheria, such as Bovidae and Equidae in tropical savanna and temperate steps (Taira, 2007).

We estimated the most reliable date of the human–chimpanzee speciation event at 5.69 Ma, which is close to the estimate of ca. 6 Ma by Scally et al. (2012) but younger than ca. 7 to 8 Ma by Langergraber et al. (2012). We estimated *Homo sapiens* ssp. *Denisova* speciation event at 2.09 Ma, and *Homo sapiens neanderthalensis* speciation event at 0.95 Ma, although these ages are older than 0.77 to 1.3 and 0.32 to 0.61 by Krause et al. (2010), 0.65 to 0.97 Ma and 0.32 to 0.48 Ma by Fu et al. (2013), and 0.72 to 1.41 Ma and 0.36 to 0.46 Ma by Posth et al. (2016).

4.5. Increased base substitution rate toward the Holocene, increased biodiversity, and ultimate human generation

The insets in Figs. 1 and 2 show that the base substitution varied, and a constant molecular clock (strict clock model) was not applicable. The light red curve indicated that the base substitution rate has a small peak at approximately 55 Ma, probably reflecting the mammalian radiation event after the K-P boundary following the explosive model. Although Bininda-Emonds et al. (2007) showed diversification rates over time with a peak at 93 Ma, their estimates reflected their short fusion model.

The heavy red trendline (Figs. 1 and 2 insets) has an additional interesting character: the rate exponentially increased toward the Holocene since ca. 20 Ma. This phenomenon was first shown for primates (Ho et al., 2005), and they found that a Quaternary date calibration produced a faster rate than an older date calibration. BEAST v1. X can run simultaneously by applying multiple calibration points, but they employed BEAST v1. 3 (Drummond and Rambaut, 2003) that needed to run repeatedly by applying a date at every calibration point. Note that we instantaneously calibrated by multiple dates, including older dates such as the Jurassic as well as younger dates of the Quaternary, not solely calibrated by the Quaternary date, and the reason for the increasing rate is unrelated only to the Quaternary calibration. Additionally, note that combined gene analyses were not possible in the old versions of BEAST, and such users needed to discuss the rate for every gene. Therefore, although their trendlines and the equations are

similar to ours, their timetrees do not actually reflect drastic changes in base substitution rates over time but assume a constant rate as if the clock is strict.

Scally et al. (2012) suggested that the rate was decreased for Hominidae reversal in our analyses, but they pointed out that the evolution was accelerated for African Hominidae. Human timetree calibrated by radiometric carbon data (detection limit: ca. 60 kyr) suggested that the base substitution rate was approximately 1.6-fold higher than that of the older fossil-calibrated tree (Fu et al., 2013), similar to high estimate rates obtained in studies of pedigrees and laboratory mutation-accumulation lines (Ho et al., 2011).

An exponentially increased base substitution rate may be expected to increase biodiversity, as shown by the diversified species in Fig. 1. Species diversity might have been a consequence of extensive adaptive radiation triggered by the expansion of C4 grasses, effective decreases in atmospheric CO2 concentrations, global cooling, and severe climatic changes at the start of the Quaternary glacial-interglacial cycle. We moreover suspect that the ultimate effect might be the birth of *Homo* species.

5. Conclusion

Maximum ages not strictly defined in MCMCTree are practically substituted by multiple node calibrations in BEAST v.1 X. The robustly dated tree showed the evolutionary history with a series of global events of the post 70 Ma vicariant speciation between Afrotheria (Africa) and Xenarthra (South America) by progressed spreading of the Atlantic Ocean, the post K-Pg (66 Ma) placentalian radiation, post 20 Ma expansion of C4 grasses, its triggered increase carbon fixation, decrease of atmospheric CO2, global cooling, the Quaternary glacial-interglacial cycle, extensive adaptive radiation, exponentially increased base substitution (mutation) rate, and ultimately creating *Homo sapiens*.

Declarations

Acknowledgments

We thank Jen-Zon Ho (Endemic Species Research Institute, Taiwan, deceased 2018) and Yuichi Oba for their encouragement of our projects.

Disclosure statement

No conflict of interest was reported by the authors.

Funding

This research was partly supported by Grants-in-Aid for Scientific Research Japan, “Extrusion Wedge of the Sambagawa High P-T Metamorphic Rocks,” grant number 20540441.

Ethical approval

Whole mitochondrial sequence data applied, including *Homo sapiens*, were from GenBank / DDBJ, and not ours.

References

Archibald JD, Deutschman D. 2001. Quantitative analysis of the timing of the origin and diversification of extant placental orders. Journal of Mammalian Evolution 8: 107–124.

Bacon CD, Silvestro D, Jaramillo C, Smith BT, Chakrabarty P, Antonell A. 2015. Biological evidence supports an early and complex emergence of the Isthmus of Panama. Proceedings of National Academy of Sciences, USA 112: 6110–6115.

Badgley C, Barry JC, Morgan ME, Nelson SV, Behrensmeyer AK, Cerling TE, Pilbeam D. 2008. Ecological changes in Miocene mammalian record show impact of prolonged climatic forcing. Proceedings of the National Academy of Sciences, USA 105: 12145–12149.

Bajpai, S. and Gingerich, P.D. 1998. A new Eocene archaeocete (Mammalia, Cetacea) from India and the time of origin of whales. Proceedings of the National Academy of Sciences, USA 95: 15464-15468.

Barnett-Moore N, Mu€ller DR, Williams S, Skogseid J, Seton M. 2018. A reconstruction of the North Atlantic since the earliest Jurassic. Basin Research 30: 160–185.

Barry, J.C., Morgan, M.L.E., Flynn, L.J., Pilbeam, D., Behrensmeyer, A.K., Raza, S.M., Khan, I.A., Badgley, C., Hicks, J., and Kelley, J. 2002. Faunal and environmental change in the late Miocene Siwaliks of northern Pakistan. Paleobiology 28: 1-71.

Benton MJ, Donoghue PCJ. 2007. Paleontological evidence to date the tree of life. Molelular Biology and Evolution 24: 26–53.

Benton MJ, Donoghue PCJ, Asher RJ, Friedman MN, Near TJ, Vinther J. 2015. Constraints on the timescale of animal evolutionary history. Palaeontologia Electronica 18.1.1FC; 1-106.

Berta P, Hawkins JR, Sinclair AH, Taylor A, Griffiths BL, Goodfellow PN, Fellous M. 1990. Genetic evidence equating SRY and the testis-determining factor. Nature 348: 448–450.

Bertrand A, Rosenberg C, Rabaute A, Herman F, Fügenschuh B. 2017. Exhumation mechanisms of the Tauern Window (Eastern Alps) inferred from apatite and zircon fission track thermochronology. Tectonics 36: 207-228.

Bloch JI, Silcox MT, Boyer DM, Sargis EJ. 2007. New Paleocene skeletons and the relationship of plesiadapiforms to crown-clade primates. Proceedings of the National Academy of Sciences, USA 104: 1159-1164.

Bininda-Emond ORP, Cardillo M, Jones KE, MacPhee RDE, Beck RMD, Grenyer R, Price SA, Vos RA, Gittleman JL, Purvis A. 2007. The delayed rise of present-day mammals. Nature 446: 507–512.

Blaise S, de Parseval N, Benit L, Heidmann T. 2003. Genomewide screening for fusogenic human endogenous retrovirus envelopes identifies syncytin 2, a gene conserved on primate evolution. Proceedings of the National Academy of Sciences, USA 100: 13013–13018.

Bouckaert R, Heled J, Kuhnert D, Vaughan T, Wu CH, Xie D, et al. 2014. BEAST 2: A software platform for Bayesian evolutionary analysis. Computational Biology 10: e1003537. doi: 10.1371/journal.pcbi.1003537

Brower AVZ. 1994. Rapid morphological radiation and convergence among races of the butterfly *Heliconius erato* inferred from patterns of mitochondrial DNA evolution. Proceedings of the National Academy of Sciences of the United States of America 91: 6491-6495.

Buchs DM, Irving D, Coombs H, Miranda R, Wang J, Coronado M, Arrocha R, Lacerda M, Goff C, Almengor E, Portugal E, Franceschi P, Chichaco E, Redwood SD. 2019. Volcanic contribution to emergence of Central Panama in the Early Miocene. Scientific Reports 9, 1417.

Caceres M, Comparative N, Program S, Thomas JW. 2006. The Gene of retroviral origin Syncytin 1 is specific to Hominoids and is inactive in Old World monkeys. Journal of Heredity 97: 100–106.

Cerling TE, Harris JM, MacFadden BJ, Leakey MG, Quade J, Eisenmann V, Ehleringer JR. 1997. Global vegetation change through the Miocene / Pliocene boundary. Nature 389: 153- 158.

Cowan RJ, Searle MP, D. Waters J. 2014. Structure of the metamorphic sole to the Oman Ophiolite, Sumeini Window and Wadi Tayyin: implications for ophiolite obduction processes. In Rollinson HR, Searle MP, Abbasi IA, Al-Lazki A. Al-Kindi MH (eds) Tectonic Evolution of the Oman Mountains, Geological Society, London, Special Publications 392: 155–175.

Deino AL, Tauxe L, Monaghan M, Hill A. 2002. 40Ar/(39)Ar geochronology and paleomagnetic stratigraphy of the Lukeino and lower Chemeron Formations at Tabarin and Kapcheberek, Tugen Hills, Kenya. Journal of Human Evolution 42: 117-140.

Donoghue PCJ, Yang Z. 2016. The evolution of methods for establishing evolutionary timescales. Philosophical Transactions of the Royal Society B. 371: 20160020. doi:10.1098/rstb.2016.0020

dos Reis M, Inoue J, Hasegawa M, Asher RJ, Donoghue PCJ, Yang Z. 2012. Phylogenomic datasets provide both precision and accuracy in estimating the timescale of placental mammal phylogeny. Proceedings of the Royal Society B 279, 3491–3500. doi:10.1098/rspb.futougou 2012.0683

dos Reis M, Gunnell GF, Barba-Montoya J, Wilkins A, Yang Z, Yoder AD. 2018. Using phylogenomic data to explore the effects of relaxed clocks and calibration strategies on divergence time estimation: primates as a test case. Systematic Biology 67: 594–615.

Drummond, A. J., and A. Rambaut. 2003. BEAST. Version 1.3. Oxford University Press, Oxford. http://evolve.zoc.ox.ac.uk/beast/

Drummond AJ, Suchard MA, Xie D, Rambaut A. 2012. Bayesian phylogenetics with BEAUti and the BEAST 1.7. Molecular Biology and Evolution 29: 1969-1973.

Dupressoir A, Laviallea C, Heidmann T. 2012. From ancestral infectious retroviruses to bona fide cellular genes: Role of the captured syncytins in placentation. Placenta 33: 663-671.

Farris DW, Jaramillo C, Bayona G, Restrepo-Moreno SA, Montes C, Cardona A, Mora A, Speakman RJ, Glascock MD, Victor Valencia V. 2011. Fracturing of the Panamanian Isthmus during initial collision with South America. Geology 39: 1007–1010.

Farris, D. W., Cardona, A., Montes, C., Foster, D., Jaramillo, C. 2017. Magmatic evolution of Panama Canal volcanic rocks: A record of arc processes and tectonic change. PLoS One 12, e0176010 (2017).

Fu Q, Mittnik A, Johnson PLF, Bos K, Lari M, Bollongino R, Sun C, Giemsch L, Schmitz R, Burger J, Ronchitelli AM, Martini F, Cremonesi RG, Svoboda J, Bauer P, Caramelli D, Castellano S, Reich D, Paabo S, Krause J. 2013. A revised timescale for human evolution based on ancient mitochondrial genomes. Current Biology 23: 553–559.

Gabaldon T, Koonin EV. 2013. Functional and evolutionary implications of gene orthology. Nature Reviews Genetics 14: 360–366.

Grande L. 1980. Paleontology of the Green River Formation with a review of the fish fauna. The Geological Survey of Wyoming Bulletin 63: 1-333.

Gouy M, Guindon S, Gascuel O. 2010. SeaView version 4 : a multiplatform graphical user interface for sequence alignment and phylogenetic tree building. Molecular Biology and Evolution 27: 221-224.

Hassanin A, Veron G, Ropiquet A, Jansen van Vuuren B, Lecu A, Goodman SM, et al. 2021. Evolutionary history of Carnivora (Mammalia, Laurasiatheria) inferred from mitochondrial genomes. PLoS ONE 16(2): e0240770. https://doi. org/10.1371/journal.pone.0240770

He HY, Wang XL, Jin F, Zhou ZH, Wang F, Yang LK, Ding X, Boven A, Zhu RX. 2006. The 40Ar/39Ar dating of the early Jehol Biota from Fengning, Hebei Province, northern China. Geochemistry, Geophysics, Geosystems7: Q04001. doi:10.1029/2005GC001083 ISSN: 1525-2027

Ho SY, Phillips MJ, Cooper A, Drummond AJ. 2005. Time dependency of molecular rate estimates and systematic overestimation of recent divergence times. Molecular Biology and Evolution 2: 1561–1568.

Ho SY, Robert Lanfear R, Bromham L, Phillips MJ, Soubrier J, Rodrigo AG, Alan C. 2011. Time-dependent rates of molecular evolution. Molecular Ecology 20: 3087-3101. doi: 10.1111/j.1365-294X.2011.05178.x

Ho SYW, Duchene S. 2014. Molecular-clock methods for estimating evolutionary rates and timescales. Molecular Ecology 23: 5947–5965.

Horvath JE, Weisrock DW, Embry SL, Fiorentino I, Balhoff JP, Kappeler P, Wray GA, Willard HF, Yoder AD. 2008. Development and application of a phylogenomic toolkit: Resolving the evolutionary history of Madagascar's lemurs. Genome Research 18: 489-499.

Houle A. 1999. The Origin of Platyrrhines: An evaluation of the Antarctic scenario and the floating island model. American Journal of Physical Anthropology 109:541–559.

Johnson NM, Stix J, Tauxe L, Cerveny PF, Tahirkheli RAK. 1985. Paleomagnetic chronology, fluvial processes, and tectonic implications of the Siwalik deposits near Chinji Village, Pakistan. Journal of Geology 93: 27-40.

Katoh S, Beyene Y, Itaya T, Hyodo H, Hyodo M, Yagi K, Gouzu C, WoldeGabriel G, Hart WK, Ambrose SH, Nakaya, Bernor RL, Boisserie JR, Bibi F, Saegusa H, Sasaki T, Sano K, Asfaw B, Suwa G. 2016. New geological and palaeontological age constraint for the gorilla–human lineage split. Nature 530: 215-218.

Krause J, Fu Q, Good JM, Viola B, Shunkov MV, Derevianko AP, Paabo S. 2010. The complete mitochondrial DNA genome of an unknown hominin from southern Siberia. Nature 464. doi:10.1038/nature08976

Kriegs JO, Churakov G, Kiefmann M, Jordan U, Brosius J, Schmitz J. 2006. Retroposed Elements as Archives for the Evolutionary History of Placental Mammals. PLoS Biology 4: e91. doi:10.1371/journal.pbio.0040091

Lagabrielle Y, Goddéris Y, Donnadieu Y, Malavieille J, Suarez M. 2009. The tectonic history of Drake Passage and its possible impacts on global climate. Earth and Planetary Science Letters 279 197–211.

Lanfear R, Frandse, PB, Wright AM, Senfel T, Calcott B. 2016. PartitionFinder 2: new methods for selecting partitioned models of evolution for molecular and morphological phylogenetic analyses. Molecular Biology and Evolution. doi: dx.doi.org/10.1093/molbev/msw260

Langergraber KE. et al. 2012. Generation times in wild chimpanzees and gorillas suggest earlier divergence times in great ape and human evolution. Proceedings of the National Academy of Sciences, USA 109: 15716–15721.

Liu L, Zhang J, Rheindt FE, Lei F, Qu Y, Wang Y, Zhang Y, Sullivan C, Nie W, Wang J, Yang F Chen J, Edwards SV, Meng J, Wu S. 2017. Genomic evidence reveals radiation of placental mammals uninterrupted by the KPg boundary. Proceedings of the National Academy of Sciences, USA 114: E7282-E7290 (2017). doi: 10.1073/pnas.1616744114

Luo ZX, Wible JQ, Yuan CX. 2003. An Early Cretaceous tribosphenic mammal and metatherian evolution. Science 30: 1934-1940.

Luo ZX, Yuan CX, Meng QJ, Ji Q. 2011. A Jurassic eutherian mammal and divergence of marsupials and placentals. Nature 476:442-445.

Magallon S, Gomez-Acevedo S, Sanchez-Reyes LL, Hernandez-Hernandez T. 2015. A metacalibrated time tree documents the early rise of flowering plant phylogenetic diversity. New Phytologist 207: 437–453.

McKenna DD, et al. 2015. The beetle tree of life reveals that Coleoptera survived end-Permian mass extinction to diversify during the Cretaceous terrestrial revolution. Systematic Entomology 40: 835–880.

Martill DM. 2007. The age of the Cretaceous Santana Formation fossil Konservat Lagerstatte of north-east Brazil: a historical review and an appraisal of the biochronostratigraphic utility of its palaeobiota. Cretaceous Research 28: 895-920.

McBrearty S, Jablonski NG. 2005. First fossil chimpanzee. Nature 437. doi:10.1038/nature04008

Meredith RW et al. 2011. Impacts of the Cretaceous terrestrial revolution and KPg extinction on mammal diversification. Science 334, 521-524.

Montes C, Cardona A, Jaramillo C, Pardo A, Silva C, Valencia V, C. Ayala C, Perez-Angel JC, Rodriguez-Parra LA, Ramirez V, Nino H. 2015. Middle Miocene closure of the Central American Seaway. Science 348: 226-229.

Moulin M, Aslanian D, Unternehr P. 2010. A new starting point for the south and equatorial Atlantic Ocean. Earth-Science Reviews 98: 1–37.

Murphy WJ, Eizirik E, O'Brien SJ, Madsen O, Scally M, Douady CJ, Teeling E, Ryder OA, Stanhope MJ, de Jong WW, Springer MS. 2001. Molecular phylogenetics and the origins of placental mammals. Nature 409: 614-618.

Nishihara H, Maruyama S, Okada N. 2009. Retroposon analysis and recent geological data suggest near-simultaneous divergence of the three superorders of mammals. Proceedings of the National Academy of Sciences of the USA 106: 5235–5240.

Nilsson MA, Churakov G, Sommer M, Tran NV, Zemann A, et al. 2010. Tracking marsupial evolution using archaic genomic retroposon insertions. PLoS Biol 8(7): e1000436. doi:10.1371/journal.pbio.1000436

Oba Y, Konishi K, Yano D, Shibata H, Kato D, Shirai T. 2020. Resurrecting the ancient glow of the fireflies. Science Advances 6, eabc5705.

O'Leary MA, Bloch JI,Flynn JJ, Gaudin TJ, Giallombardo A, Giannini NP, Suzann L. Goldberg SL, Kraatz BP, Luo ZX, Meng J, Ni X, Novacek MJ, Perini FA, Randall ZS, Rougier GW, Sargis EJ, Mary T. Silcox MT, Nancy B. Simmons NB, Spaulding M, Velazco PM, Marcelo Weksler MW, John R. Wible JR, Andrea L. Cirranello AL. 2013. The Placental mammal ancestor and the post–K-Pg radiation of Placentals. Science 339, 662-667. doi: 10.1126/science.1229237

Osozawa K, Ogino S, Osozawa S, Oba Y, Wakabayashi J. 2016. Carabid beetles (Carabus blaptoides) from Nii-jima and O-shima isles, Izu-Bonin oceanic islands: dispersion by Kuroshio current and the origin of the insular populations. Insect Systematics and Evolution 47: 1–16.

Osozawa S. 2021. BEAST v1.X tutorial: Mammalian timetree. protocols.io. dx.doi.org/10.17504/protocols.io.brdym27w

Osozawa S, Wakabayashi J. 2015. Killer typhoons began to impact the Japanese islands from ca.1.55 Ma, based on phylogeography of Chlorogomphus (gliding dragonfly). Journal of Earth Science and Climatic Change S3:003. doi: 10.4172/2157-7617.S3-003

Osozawa S, Shinjo R, Armig R, Watanabe Y, Horiguchi T, Wakabayashi J. 2012a. Palaeogeographic reconstruction of the 1.55 Ma synchronous isolation of the Ryukyu Islands, Japan, and Taiwan and inflow of the Kuroshio warm current. International Geology Review54: 1369-1388.

Osozawa, S., Shinjo, R., Lo, C.H., Jahn, B., Hoang, N., Sasaki, M., Ishikawa K., Kano, H., Hoshi, H., Xenophontos, C., Wakabayashi, J., 2012b. Geochemistry and geochronology of the Troodos ophiolite: An SSZ ophiolite generated by subduction initiation and an extended episode of ridge subduction? Lithosphere 4: 497–510.

Osozawa S, Su ZH, Oba Y, Yagi T, Watanabe Y, Wakabayashi J. 2013. Vicariant speciation due to 1.55 Ma isolation of the Ryukyu islands, Japan, based on geological and GenBank data. Entomological Science 16: 267-277.

Osozawa S, Takáhashi M, Wakabayashi J. 2015a. Ryukyu endemic Mycalesis butterflies, speciated vicariantly due to isolation of the islands since 1.55 Ma. Lepidoptera Science 66: 8-14.

Osozawa S, Oba Y, Kwon HY, Wakabayashi J. 2015b. Vicariance of Pyrocoelia (Lampyridae; firefly) in the Ryukyu islands, Japan. Biological Journal of the Linnean Society 116: 412-422.

Osozawa S, Vuong NV, Tich VV, Wakabayashi J. 2015. Reactivation of a collisional suture by Miocene transpressional domes associated with the Red River and Song Chay detachment faults, northern Vietnam. Journal of Asian Earth Sciences 105: 252-269.

Osozawa S, Fukuda H, Kwon HY, Wakabayashi J. 2016. Quaternary vicariance of tiger beetle, Cicindela chinensis, in Ryukyu, Japan, Taiwan and Korea–China. Entomological Research 46; 122–127.

Osozawa S, Takáhashi M, Wakabayashi J. 2017a. Quaternary vicariance of Ypthima butterflies (Lepidoptera, Nymphalidae, Satyrinae) and systematics in the Ryukyu Islands and Oriental region. Zoological Journal of the Linnean Society 180: 593-602.

Osozawa S, Shiyake S, Fukuda H, Wakabayashi J. 2017b. Quaternary vicariance of Platypleura (Cicadidae) in Japan, Ryukyu, and Taiwan islands. Biological Journal of the Linnean Society 121: 185-199. doi: https://doi.org/10.1093/biolinnean/blw023

Osozawa S, Sato F, Wakabayashi J. 2017c. Quaternary vicariance of lotic Coeliccia in the Ryukyu-Taiwan islands contrasted with lentic Copera. Journal of Heredity 108: 280-287.

Osozawa S, Kanai K, Fukuda H, and Wakabayashi J, 2021a. Wakabayashi J (2021) Phylogeography of Ryukyu insular cicadas: Extensive vicariance by island isolation vs accidental dispersal by super typhoon. PLoS ONE 16(5): e0244342. https://doi.org/ 10.1371/journal.pone.0244342

Osozawa S, Nakejima C, Wakabayashi J. 2021b. Post-Triassic Spermatophyta timetree adding the Quaternary radiated *Asarum* wild gingers. Research Square. doi 10.21203/rs.3.rs-99466/v1

Phillips MJ. 2011. Geomolecular dating and the origin of placental mammals. Systematic Biology 65: 546–557.

Pindell J, Maresch WV, Martens U, Stanek K. 2011. The Greater Antillean Arc: Early Cretaceous origin and proposed relationship to Central American subduction mélanges: implications for models of Caribbean evolution. International Geology Review 54: 131-143.

Posth C, Wi□ing C, Kitagawa K, Pagani L, van Holstein L, Racimo F, Wehrberger K, Conard NJ, Kind CJ, Bocherens H, Krause J. 2016. Deeply divergent archaic mitochondrial genome provides lower time boundary for African gene flow into Neanderthals. Nature Communications 8: 16046. doi: 10.1038/ncomms16046

Pozzi L, Hodgson JA, Burrell AS, Sterner KN, Raaum RL, Disotell TR. 2014. Primate phylogenetic relationships and divergence dates inferred from complete mitochondrial genomes. Molecular Phylogenetics and Evolution 75: 165–183.

Rezaei F, Azizi H, Asahara Y. 2021. Tectonic significance of the late Eocene (Bartonian) calc-alkaline granitoid body in the Marivan area, Zagros suture zone, northwest Iran. International Geology Review. doi: 10.1080/00206814.2021.1907624

Riley TR, Carter A, Leat PT, Burton-Johnson A., Bastias J, Spikings RA, Tate AJ, Bristow CS, 2019. Geochronology and geochemistry of the northern Scotia Sea: A revised interpretation of the North and West Scotia ridge junction. Earth and Planetary Science Letters 518: 136–147.

Roberts, E.M., O'Connor, P.M., Stevens, N.J., Gottfried, M.D., Jinnah, Z.A., Ngasala, S., Choh, A.M., Armstrong, R.A. 2010. Sedimentology and depositional environments of the Red Sandstone Group, Rukwa Rift Basin, southwestern Tanzania: New insight into Cretaceous and Paleogene terrestrial ecosystems and tectonics in sub-equatorial Africa. Journal of African Earth Sciences 57: 179-212.

Roberts EM, Stevens NJ, O'Connor PM, Dirks PHGM, Gottfried MD, Clyde WC, Armstrong RA, Kemp AIS Hemming S. 2010. Initiation of the western branch of the East African Rift coeval with the eastern branch. Nature Geoscience **5**. doi: 10.1038/NGEO1432

Robinson, P., Gunnell, G.F., Walsh, S.L., Clyde, W.C., Storer, J.E., Stucky, R.K., Froehlich, D.J., Ferrusquia-Villafranca, I., and McKenna, M.C. 2004. Wasatchian through Duchesnean biochronology, p. 106-155. In Woodburne, M.O. (ed.), Late Cretaceous and Cenozoic mammals of North America: Biostratigraphy and geochronology. Columbia University Press, New York.

Rose, K.D., DeLeon, V.B., Missiaen, P., Rana, R.S., Sahni, A., Singh, L., Smith, T. 2008. Early Eocene lagomorph (Mammalia) from Western India and the early diversification of Lagomorpha. Proceedings of the Royal Society, Series B **275**: 1203-1208.

Rioux M, Garber JM, Searle M, Kelemen P, Miyashita S, Adachi Y, Bowring S. 2021. High-precision U-Pb zircon dating of late magmatism in the Samail ophiolite: A record of subduction initiation. JGR Solid Earth. doi: 10.1029/2020JB020758

Sahney S, Benton MJ, Ferry PA. 2010. Links between global taxonomic diversity, ecological diversity and the expansion of vertebrates on land. Biology Letters. doi:10.1098/rsbl.2009.1024

Scally A. et al. 2012. Insights into hominid evolution from the gorilla genome sequence. Nature 483: 169-175.

Searl MP, Godin L. 2003. The South Tibetan Detachment and the Manaslu leucogranite: A structural reinterpretation and restoration of the Annapurna-Manaslu Himalaya, Nepal. The Journal of Geology 111: 505–523.

Sepulchre P, Ramstein G, Fluteu F, Mathieu Schuster M, Tiercelin JJ, Brunet M. 2006. Tectonic uplift and eastern Africa aridification. Science 313: 1419-1423.

Springer MS, Foley NM, Brady PL, Gatesy J and Murphy WJ. 2019. Evolutionary models for the diversification of placental mammals across the KPg boundary. Frontiers in Genetics 10: 1241. doi: 10.3389/fgene.2019.01241

Smith ME, Singer B, Carroll A. 2003. 40 Ar/39 Ar geochronology of the Eocene Green River Formation, Wyoming. Geological Society of America Bulletin 115: 549–565.

Stecher G, Tamura K, Kumar S. 2020. Molecular Evolutionary Genetics Analysis (MEGA) for macOS. Molecular Biology and Evolution. doi.org/10.1093/molbev/msz312

Stevens NJ, Seiffert ER, O'Connor PM, Roberts EM, Schmitz MD, Krause C, Gorscak E, Ngasala S, Tobin L. Hieronymus TL, Temu J. 2013. Palaeontological evidence for an Oligocene divergence between Old World monkeys and apes. Nature 497: 611-614.

Suchard, M.A., Lemey, P., Baele, G., Ayres, D.L., Drummond, A.J., Rambaut, A. 2018. Bayesian phylogenetic and phylodynamic data integration using BEAST 1.10. Virus Evolution 4: vey016.

Taira A. 2007. Search the Earth History, Geology 3, pp. 396. Iwanami Shoten, Publishers, Tokyo. (in Japanese)

Thorne JL, Kishino H. 2002. Divergence time and evolutionary rate estimation with multilocus data. Systematic Biology 51: 689–702.

Turner AH, Pritchard AC, Matzke NJ. 2017. Empirical and Bayesian approaches to fossil-only divergence times: A study across three reptile clades. PLoS ONE 12(2): e0169885. doi:10.1371/journal.pone.0169885

Vignaud P, Duringer P, Mackaye HT, et al. (21 co-authors). 2002. Geology and palaeontology of the Upper Miocene Toros- Menalla hominid locality, Chad. Nature 418: 152–155.

Waku D, Segawa T, Yonezawa T, Akiyoshi A, Ishige T, Ueda M, Ogawa H, Sasaki H, Ando M, Kohno N, Takeshi Sasaki T. 2016. Evaluating the phylogenetic status of the extinct Japanese otter on the basis of mitochondrial genome analysis. PLoS One 3;11(3):e0149341. doi: 10.1371/journal.pone.0149341.

Wu J, Yonezawa T, Kishino H. 2017. Rates of molecular evolution suggest natural history of life history traits and a post-K-Pg nocturnal bottleneck of placentals. Current Biology 27: 3025–3033.

Yang Z. 2007. PAML 4: phylogenetic analysis by maximum likelihood. Molecular Biology and Evolution 24, 1586 – 1591. doi:10.1093/molbev/msm088

Table

Due to technical limitations, Table 1 is only available as a download in the supplemental files section

Figures

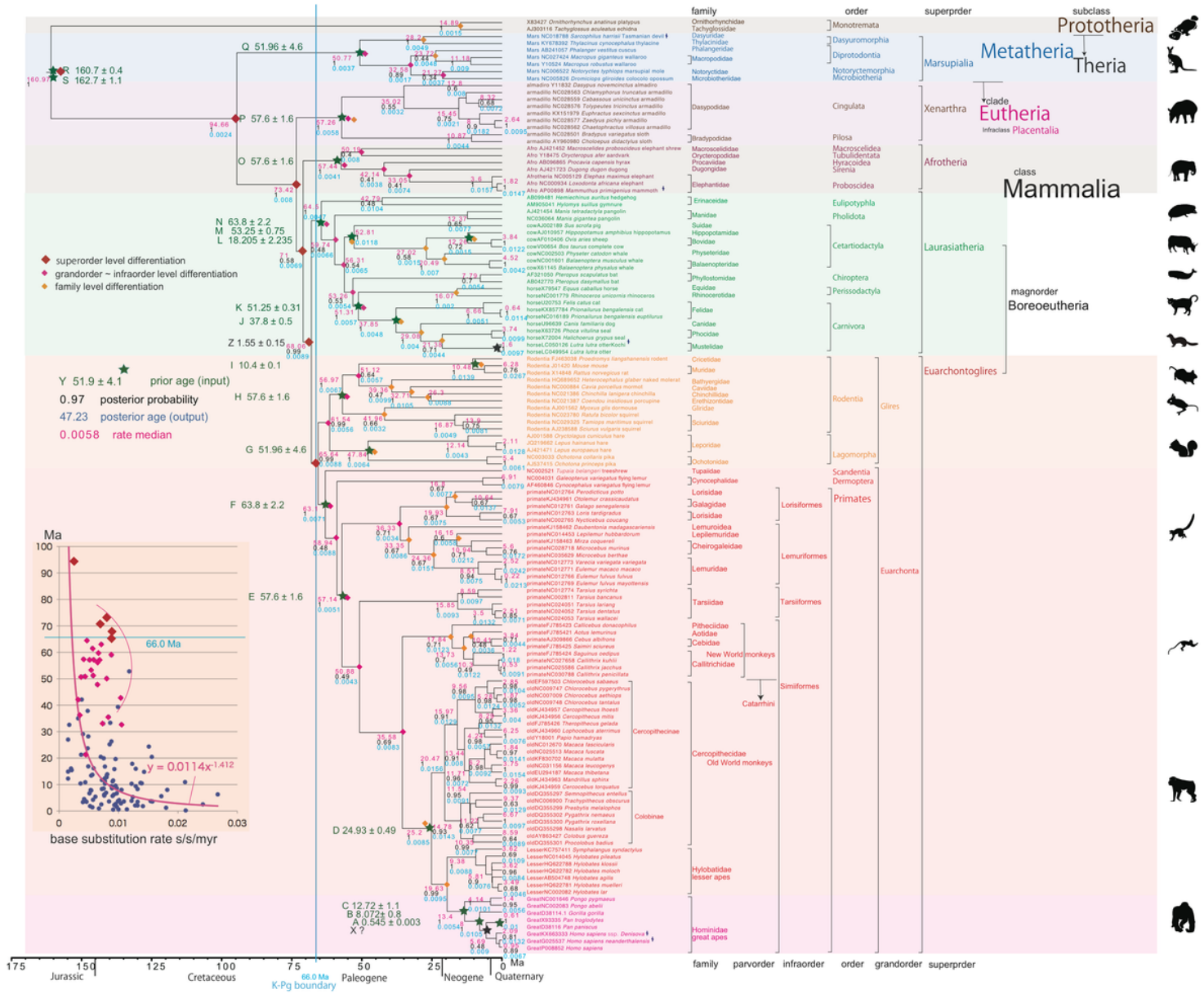

Figure 1

Mammalian timetree built by BEAST v1. X. Fossil calibrations from A to S were solely by minimum ages. The Pan-Homo splitting date was not calibrated but expressed X and was estimated at 5.69 Ma. Geological event calibration: point Z. Ordinal differentiation was a post K-Pg boundary event. Illustrations were downloaded from silhouette AC. Inset: Base substitution rate (= rate median shown at each node; mutations per bp per million years) vs age (= posterior age shown at each node) diagram. Heavy red curve with equation: trendline drawn by Excel function, and light red curve: trendline drawn by connecting plots with maximum rate through the time.

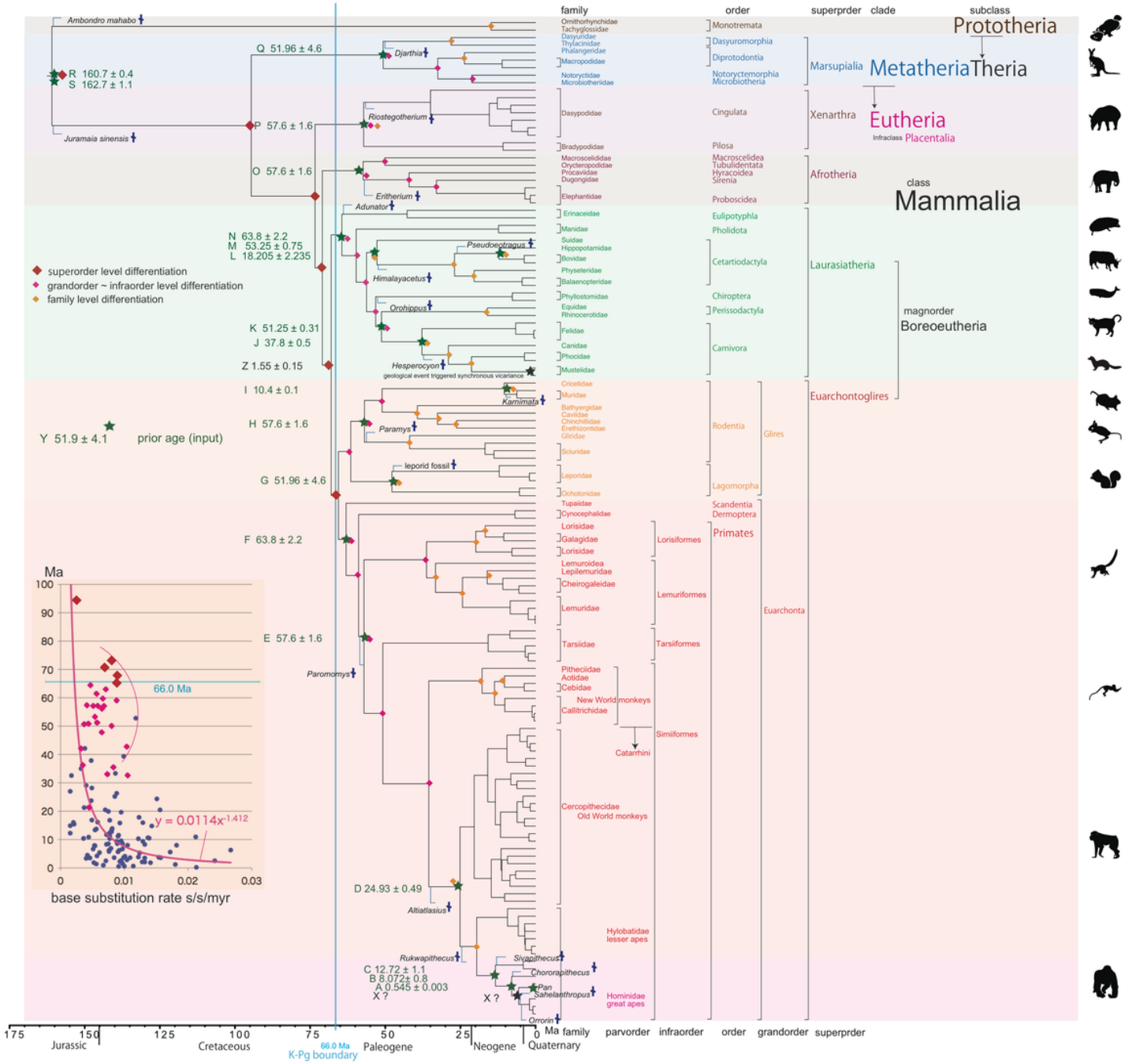

Figure 2

Mammalian timetree built by BEAST v1. X, implified from Fig. 1. Fossils with cross marks to adjust minimum ages (Benton et al., 2015) were shown close to each calibration point.

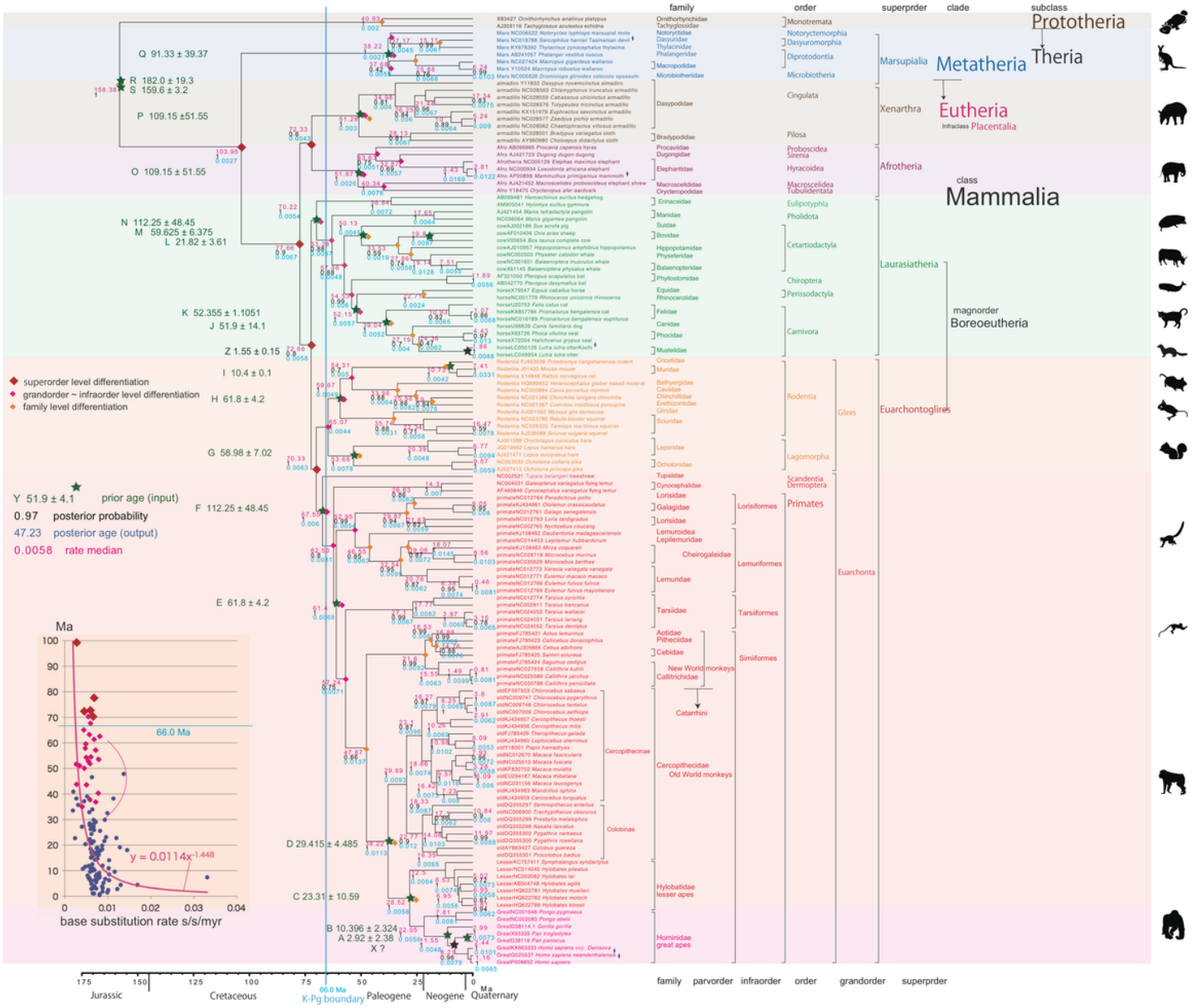

Figure 3

Mammalian timetree built by BEAST v1. X. Prior distribution: normal. Fossil calibrations from A to S were calculated by considering maximum ages in addition to minimum ages. The Pan-Homo splitting date was not calibrated but expressed X and was estimated at 8.79 Ma. Geological event calibration: point Z. Ordinal differentiation was a post K-Pg boundary event with an exception. Illustrations were downloaded from silhouette AC. Inset: Base substitution rate vs age diagram. Heavy red curve with equation: trendline drawn by Excel function, and light red curve: trendline drawn by connecting plots with maximum rate through the time.

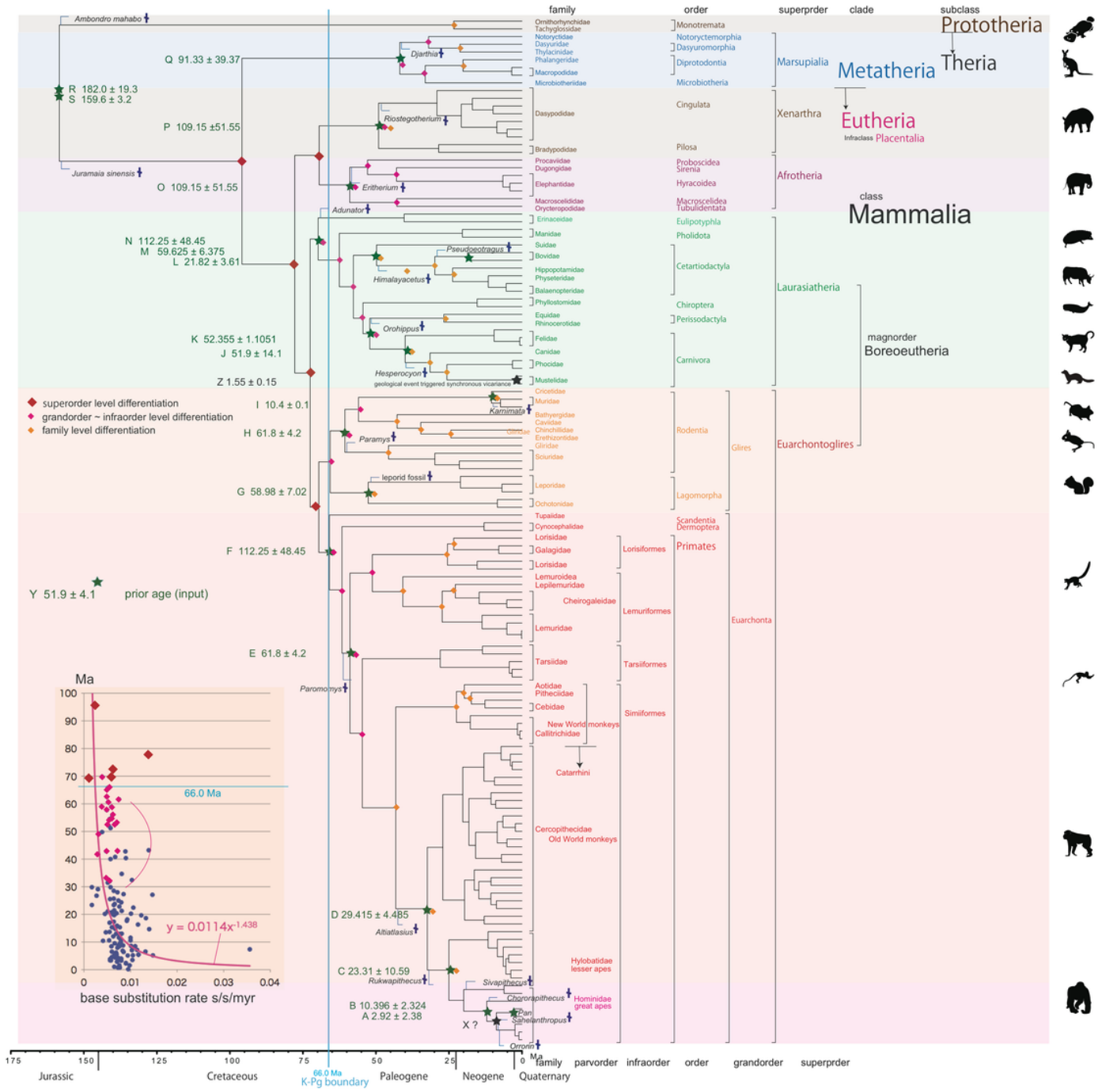

Figure 4

Mammalian timetree built by BEAST v1. X, simplified from Fig. 3. Fossils with cross marks to adjust minimum ages (Benton et al., 2015) were shown close to each calibration point.

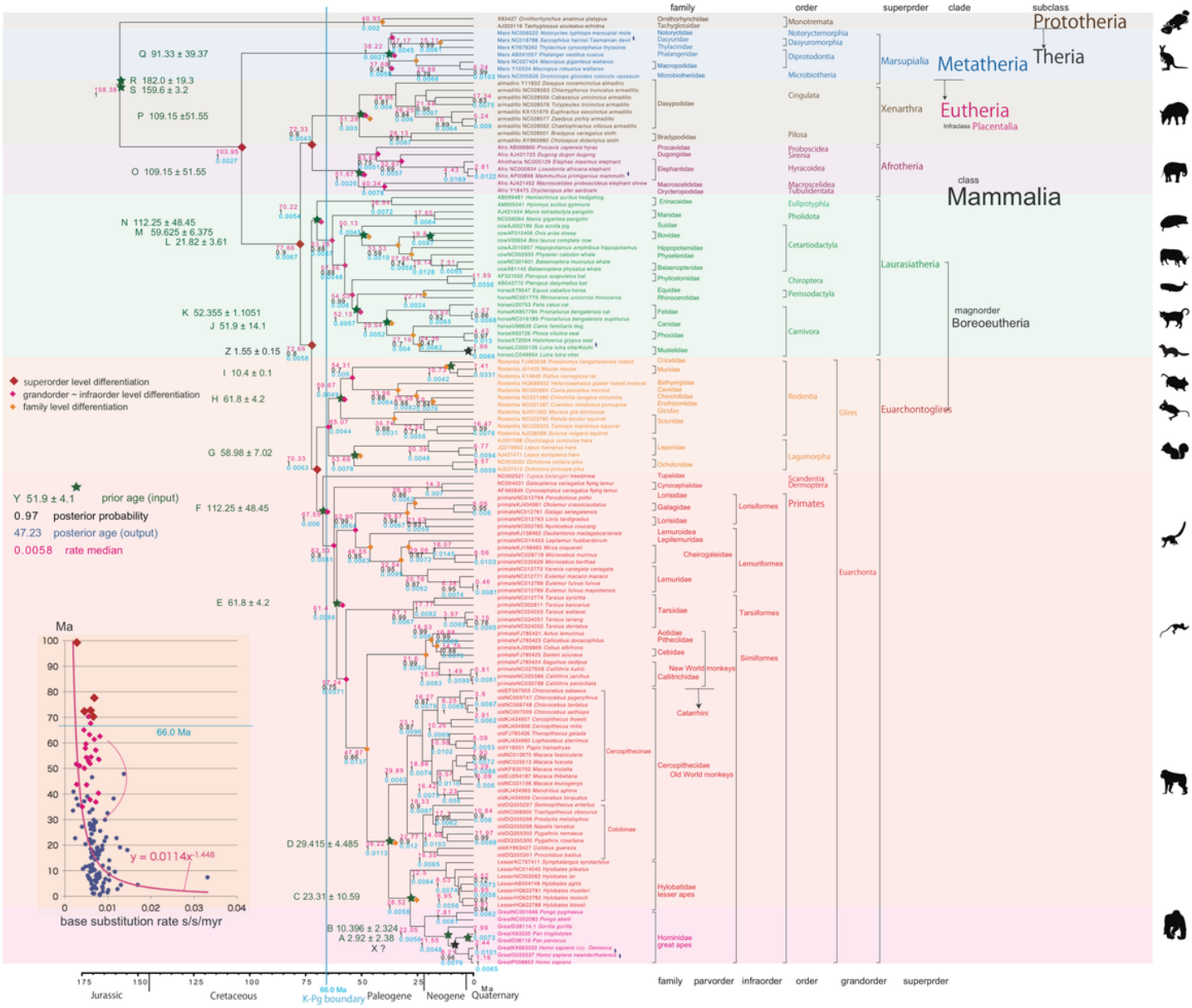

Figure 5

Mammalian timetree built by BEAST v1. X, similar to Fig. 3, except for the prior distribution: lognormal. The Pan-Homo splitting date was not calibrated but expressed X and estimated at 8.21 Ma.

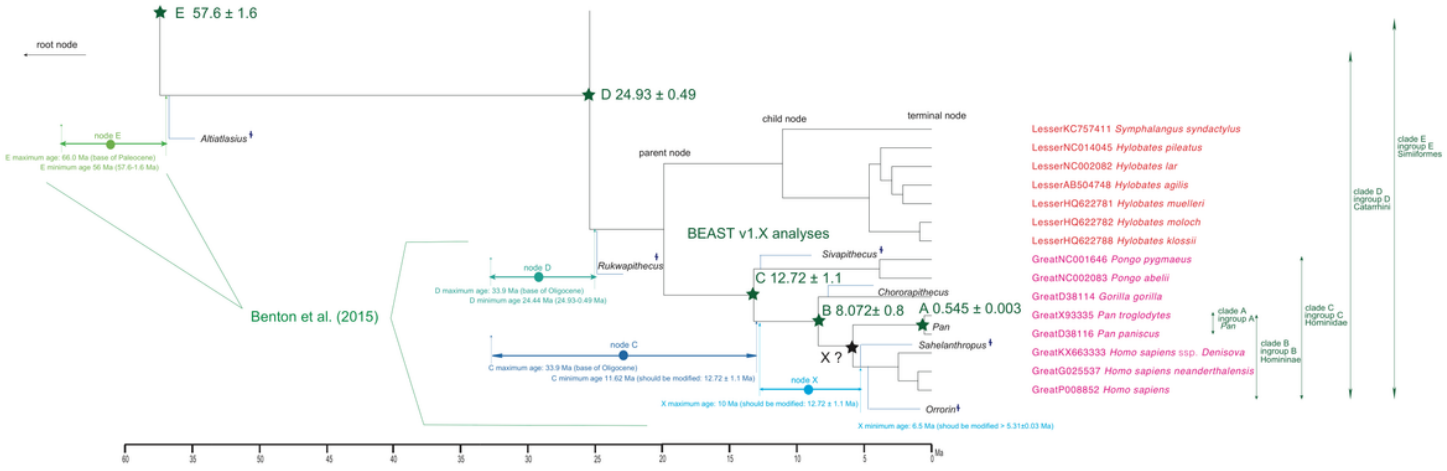

Figure 6

Comparison calibration ages for Simiiformes. Our calibrated nodes approximated the minimum ages, and those by Benton et al. (2015) approximated between maximum and minimum ages with wide ranges. Our node B age is at 8.072± 0.8 Ma, but the maximum age can be automatically constrained by its parent node C age at 12.72 ± 1.1 Ma. Node C maximum age should be replaced by node D minimum age, and this definition of maximum age is inappropriate. From nodes E to Q, maximum ages are mostly difficult to assign and overestimated by Benton et al. (2015).

Supplementary Files

This is a list of supplementary files associated with this preprint. Click to download.

- BEASYvsMCMC.png